

Conductivity noise across temperature driven transitions of rare-earth nickelate heterostructures

Gopi Nath Daptary,¹ Siddharth Kumar,¹ M. Kareev,² J. Chakhalian,² Aveek Bid,^{1,*} and S. Middey^{1,†}

¹*Department of Physics, Indian Institute of Science, Bengaluru 560012, India*

²*Department of Physics and Astronomy, Rutgers University, Piscataway, New Jersey 08854, USA*

The metal-insulator transition (MIT) of bulk rare-earth nickelates is accompanied by a simultaneous charge ordering (CO) transition. We have investigated low-frequency resistance fluctuations (noise) across the MIT and magnetic transition of [EuNiO₃/LaNiO₃] superlattices, where selective suppression of charge ordering has been achieved by mismatching the superlattice periodicity with the periodicity of charge ordering. We have observed that irrespective of the presence/absence of long-range CO, the noise magnitude is enhanced by several orders with strong non- $1/f$ (f = frequency) component when the system undergoes MIT and magnetic transition. The higher order statistics of resistance fluctuations reveal the presence of strong non-Gaussian components in both cases, further indicating inhomogeneous electrical transport arising from the electronic phase separation. Specifically, we find almost three orders of magnitude smaller noise in the insulating phase of the sample without long-range CO compared to the sample with CO. These findings suggest that digital synthesis can be a potential route to implement electronic transitions of complex oxides for device application.

I. INTRODUCTION

Metal-insulator transition (MIT), observed in complex materials as a function of temperature, chemical doping, electrostatic gating, magnetic field, light, pressure, epitaxy etc., remains a topic of paramount interest over decades^{1,2}. The complexity of the mechanism of MIT in rare earth nickelate series have attracted significant attentions in recent years^{3,4}. In the bulk form, $RENiO_3$ with RE = Sm, Eu, Lu, Y etc. undergoes a first order transition from an orthorhombic, metallic phase without charge ordering to a monoclinic, insulating phase with a rock-salt type charge ordering (CO)^{5,6}. A magnetic transition (paramagnetic to E' -antiferromagnetic) occurs at a lower temperature. Moreover, four transitions appear simultaneously in bulk NdNiO₃ and PrNiO₃. In order to explain the origin of this peculiar MIT, the importance of structural transition⁷, electron correlations⁸, charge ordering^{9,10}, distribution of ligand holes^{11–16}, polaron condensation¹⁷, Fermi surface nesting^{18–20} etc. have been emphasized by different types of experimental probes and theoretical methods. Interestingly, it has been demonstrated recently that a MIT without any long-range CO and structural symmetry change can be obtained in the artificial structure of $RENiO_3$ by mismatching the periodicity of the heterostructure with the periodicity of rock-salt type CO²¹. Apart from the interest arising from the aspect of fundamental physics, $RENiO_3$ based heterostructures also show excellent potentials for electronics applications^{3,4,22–25}.

The low-frequency $1/f$ noise is not only used for semiconductor device characterizations²⁶, but also acts a powerful tool to probe exotic phenomena like electronic phase separation²⁷, structural phase transition²⁸, charge density wave²⁹, superconductor-normal state phase transition^{30,31} etc. The frequency dependence of the power spectral density (PSD) $S_R(f)$ (described later in the text) arises due to finite relaxation of the fluctuating variable. According to the central limit theorem, the fluctuation statistics of a system is Gaussian if the fluctuators are independent of each other³². However, the presence of any correlations due to magnetic, electronic, or structural interactions in the system would result in non-Gaussian statistics of time dependent fluctuations. This

information can be extracted from higher order statistics of resistance fluctuations via ‘second spectrum’^{33,34}. The phase transitions of SmNiO₃, NdNiO₃ single-crystalline films have been studied by such noise and second spectrum measurements^{35–37}. The extremely large magnitude of noise and second spectrum have been attributed to the coexistence of metal and insulator phases near the electronic transition temperature. Such $1/f$ noise study can also provide crucial information about the length scale of charge ordering as reported earlier for colossal magnetoresistive (CMR)- manganites³⁸.

In this work, we report on resistance fluctuations across the electronic and magnetic transitions of [2uc EuNiO₃/1uc LaNiO₃] (2ENO/1LNO) and [1uc EuNiO₃/1uc LaNiO₃] (1ENO/1LNO) films (uc=unit cell in pseudo-cubic notation). 1ENO/1LNO superlattice (SL) exhibits four simultaneous transitions²¹, similar to bulk NdNiO₃ and PrNiO₃. On the other hand, 2ENO/1LNO SL is a rare example, which undergoes a first-order MIT without any long-range CO and remains monoclinic in both metallic and insulating phases²¹. We have observed the random telegraphic noise (RTN) as well as non-Gaussian component (NGC) of noise near the MIT of these films, which confirms the coexistence of spatially separated metallic and insulating phases in both samples. Importantly, we have found that the energy barrier, separating these electronic phases and the associated length scale of nanoscopic phase separation are similar in both samples. However, the noise magnitude in the insulating phase of 2ENO/1LNO SL is *three-orders of magnitude smaller* compared to the corresponding noise in 1ENO/1LNO SL, suggesting that the system having MIT without long-range charge ordering would be a better candidate for practical device applications. Interestingly, the higher order statistics of resistance fluctuations (quantified as second spectrum) becomes maximum near the antiferromagnetic transition temperature (T_N) of 2ENO/1LNO SL, implying certain role of E' -magnetic ordering in opening gap in the multi-band Fermi surface.

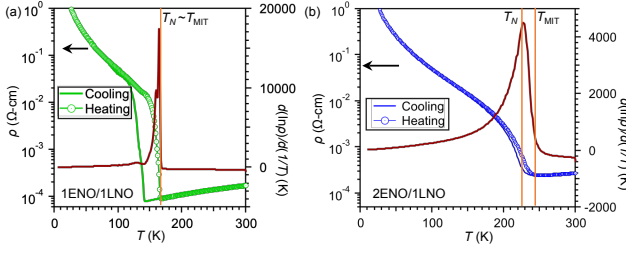


FIG. 1. Resistivity (ρ) as a function of temperature for (a) 1ENO/1LNO and (b) 2ENO/1LNO. Corresponding $d \ln(\rho)/d(1/T)$ has been also plotted as a function of T (right axis of (a) and (b)).

II. EXPERIMENTAL DETAILS

[2uc EuNiO_3 /1uc LaNiO_3] $\times 12$ (2ENO/1LNO) and [1uc EuNiO_3 /1uc LaNiO_3] $\times 18$ (1ENO/1LNO) superlattices (SLs) have been grown on single crystalline NdGaO_3 (110) substrate by pulsed laser interval deposition. The details of the growth conditions and characterizations can be found in Refs. 21, 39, and 40. The resistance and noise measurements have been performed in a cryo-free 4 K system.

III. RESULTS AND DISCUSSIONS

Figure 1(a) and (b) show the temperature dependent resistivity (ρ) for 1ENO/1LNO and 2ENO/1LNO films, respectively. From now onwards, we discuss the results of the heating run. As seen, 1ENO/1LNO and 2ENO/1LNO SLs undergo first-order insulator to metal transitions around 165 K and 245 K respectively. The magnetic transition temperatures (T_N) are found to be 165 K for 1ENO/1LNO and 225 K for 2ENO/1LNO SL from $d \ln(\rho)/d(1/T)$ vs. T plot^{39,41,42} [see right axis of Fig. 1(a) and (b)].

To probe nature of the electrical transport, we have measured low frequency resistance fluctuations of 1ENO/1LNO and 2ENO/1LNO films using standard 4 probe lock-in (LIA) technique³⁴. This technique allows to measure both the sample as well as background noise. The sample has been current biased (I) with an excitation frequency $f^* \sim 220$ Hz. The voltage fluctuations $\delta V(t)$ arise at the sideband of f^* after the signal is demodulated from the LIA. The output of the LIA has been digitized to a high speed analog to digital converter (ADC) and stored to get the time series of voltage fluctuations $\delta V(t)$. The time series of voltage fluctuations $\delta V(t)$ has been converted to time series of resistance fluctuations $\delta R(t)$ as $\delta R(t) = \delta V(t)/I$. In Fig. 2(a), we plot the time series of resistance fluctuations at different temperatures for 1ENO/1LNO SL. As clearly seen, each time series for $T > T_{\text{MIT}}$ consists of random resistance fluctuations about the average value. Similar features have been also seen in case of 2ENO/1LNO SL for $T > T_{\text{MIT}}$ (see Appendix, Fig. 5). Interestingly, we observe the appearance of random telegraphic noise (RTN) with the resistance fluctuations between two states in the temperature range 140

$\text{K} < T < 200$ K for 1ENO/1LNO SL and $200 \text{ K} < T < 260$ K for 2ENO/1LNO SL. These RTN are absent below 140 K for 1ENO/1LNO SL and 195 K for 2ENO/1LNO SL. Such RTN has been also reported for other systems e.g. manganites³⁸, and two-dimensional superconductor²⁹, where the system can fluctuate between two distinct phases. Surprisingly, the ratio of the temperature (T_{RTN}), where RTN starts to appear and the T_{MIT} is very similar (~ 0.85) for both 1ENO/1LNO and 2ENO/1LNO SLs.

To understand the origin of the RTN, we have investigated the power spectral density (PSD) of the resistance fluctuations $S_R(f)$. At each T , the resistance fluctuations have been recorded for 30 minutes. The data have been decimated and digitally filtered to eliminate 50 Hz line frequency. $S_R(f)$ has been calculated using fast Fourier transformation (FFT) technique from the filtered time series³⁴. The minimum and maximum frequency of the noise measurement are 4 mHz and 8 Hz, respectively. In order to accentuate any deviation from $1/f$ nature of the spectrum, we have plotted the quantity $f S_R(f)/R^2$ as a function of f at few representative temperatures for 1ENO/1LNO (Fig. 2(b)) and 2ENO/1LNO (Fig. 2(c)). For $T \gg T_{\text{MIT}}$, the PSD $S_R(f)$ follows $1/f^\alpha$ dependence with $\alpha \sim 1$ for both samples. However, a strong deviation from the $1/f$ dependence of the spectral power has been found within the temperature range 140 $\text{K} < T < 200$ K for 1ENO/1LNO SL and $200 \text{ K} < T < 260$ K for 2ENO/1LNO SL. Interestingly, these are the same temperature ranges, where RTN has been also observed. Further analysis shows that $S_R(f)$ in this temperature range has two components: (a) $1/f$ component, and (b) a Lorentzian term with a corner frequency f_c as

$$\frac{S_R(f)}{R^2} = \frac{A}{f} + \frac{B f_c}{f^2 + f_c^2} \quad (1)$$

The constants A and B are the measure of the relative strength of the two terms. The second term arises from single-frequency fluctuator with a frequency f_c . f_c can be extracted by the fitting (solid line) of the experimental data (symbol) using Eq. 1, as shown in Fig. 2(b) and (c) for 1ENO/1LNO and 2ENO/1LNO films, respectively for several temperatures.

The linear relation between $\ln(f_c)$ vs. $1/T$ (Fig. 2(d)) demonstrates thermally activated behavior of f_c ($f_c = f_0 e^{-E_a/k_B T}$, k_B is the Boltzmann's constant) with an activation energy $E_a \sim 0.42 \pm 0.03$ eV for both samples. Similar value of E_a was also observed in CMR manganite when it undergoes charge order transition³⁸. The physical significance of this activated behavior can be visualized as follows. For $T \ll T_{\text{MIT}}$, the entire volume is spatially insulating and the resistance fluctuations are completely random. When the temperature reaches T_{RTN} , metallic clusters start to nucleate in the insulating background. Such metastable metallic phase is separated from the insulating phase by the energy barrier E_a (upper panel of Fig. 2(e)) and the competition between these two phases results RTN in the resistance fluctuations. For $T \gg T_{\text{MIT}}$, the system is again completely in the metallic state (Fig. 2(e): lower panel) and fluctuations become random again. In the subsequent paragraphs, we discuss the results of integrated PSD and second spectrum to strengthen this pic-

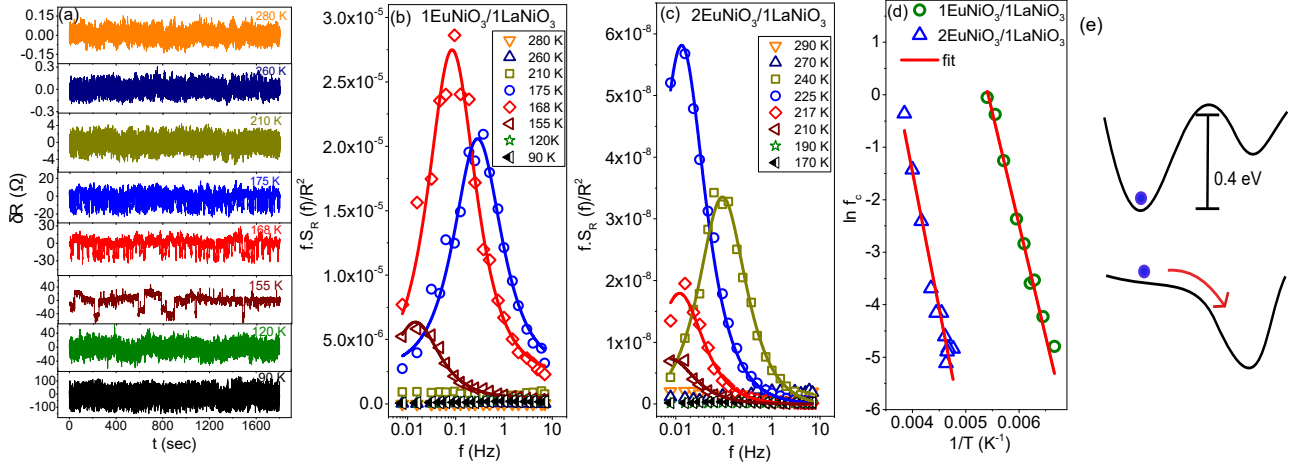


FIG. 2. (a) Time series of resistance fluctuations at few representative values of T of 1EuNiO₃/1LaNiO₃. (b) and (c) Scaled PSD of resistance fluctuations, $f S_R(f)/R^2$ as a function of frequency at a few representative values of T for 1EuNiO₃/1LaNiO₃ and 2EuNiO₃/1LaNiO₃ respectively. The solid lines are the fits to the data with Eq. 1. For details, see text. (d) Plot of f_c as a function of inverse temperature with semi-log scale. Solid lines are an Arrhenius fit to the data as discussed in the text. (e) A schematic energy diagram of two level states: insulating and metallic states. Upper and lower panel represent the position of electron (filled circle) while the system is in insulating and metallic state respectively.

ture. Details of the quantitative estimation of noise level can be found in Appendix.

The PSD of resistance fluctuations has been further integrated over the measurement bandwidth to obtain the relative variance $\frac{\delta R^2}{R^2}$ (noise) = $\frac{1}{R^2} \int S_R(f) df$. As can be seen from the inset of Fig. 3 (a) and (b), the magnitude of noise in the insulating phase of 1ENO/1LNO SL is 10^3 times larger than the observed noise in insulating phase of 2ENO/1LNO SL. The

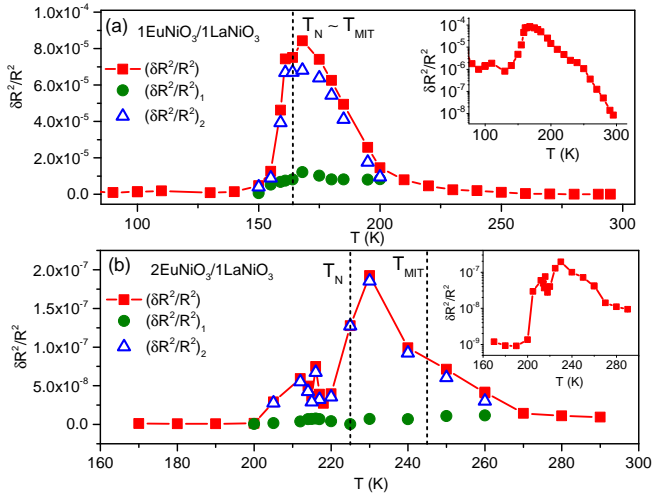


FIG. 3. (a) and (b) Temperature dependence total noise ($\delta R^2/R^2$) (red filled squares), $1/f$ noise component ($\delta R^2/R^2$)₁ (green filled circles) and Lorentzian component ($\delta R^2/R^2$)₂ (blue open triangles) of 1EuNiO₃/1LaNiO₃ and 2EuNiO₃/1LaNiO₃ respectively. For details see text. Inset in (a) and (b) shows the semi-log plot of the total noise as a function of temperatures.

noise value remains almost constant up to $T \sim 0.85 T_{MIT}$ for both samples. While the noise is maximized around $T_{MIT} \sim 165$ K for 1ENO/1LNO SL, the peak for 2ENO/1LNO SL appears around 230 K, which is 15 K lower than $T_{MIT} \sim 245$ K. Interestingly, this 2ENO/1LNO sample also shows an additional noise peak around 210 K, which is again 15 K lower than the $T_N \sim 225$ K. At this moment, the reason for this shift between the transition temperature obtained from resistivity measurement and the temperature of noise peak remains unclear. It may be related with the resistance fluctuations due to short range charge orderings⁴⁴ in insulating phase of this sample. In spite of strong difference of the noise magnitude in insulating phases of 1ENO/1LNO and 2ENO/1LNO films, noise at 300 K has similar order of magnitude ($\sim 10^{-8}$) in both samples. In the temperature range $0.85 \lesssim T/T_{MIT} \lesssim 1.1$, the total noise $\frac{\delta R^2}{R^2}$ behaves as $\frac{\delta R^2}{R^2} = \int_{f_{min}}^{f_{max}} \frac{A}{f} df + \int_{f_{min}}^{f_{max}} \frac{B f_c}{f^2 + f_c^2} df = \left(\frac{\delta R^2}{R^2} \right)_1 + \left(\frac{\delta R^2}{R^2} \right)_2$ for both samples. The temperature dependence of total noise $\frac{\delta R^2}{R^2}$, the contribution of the $1/f$ component ($\delta R^2/R^2$)₁ and Lorentzian component ($\delta R^2/R^2$)₂ are shown in Fig. 3(a) and (b). It is remarkable that noise in the temperature range $0.85 \lesssim T/T_{MIT} \lesssim 1.1$ predominantly arises from the Lorentzian component with a negligible contribution from $1/f$ term.

We note that the noise close to T_{MIT} is 2-4 orders larger than the conventional metal⁴⁵, suggesting the microstructural details of the superlattices are different from disorder metallic systems. This large increase in noise close to T_{MIT} can be due to the percolative transition of electrons in an inhomogeneous medium⁴⁶. It has been predicted for such medium from the ‘random void model’ that noise scales as R^w with $w = 2.1$. We find that $\frac{\delta R^2}{R^2} \propto R^w$ with $w \sim 2 \pm 0.1$ within the temperature range $140 \text{ K} \leq T \leq 175 \text{ K}$ for 1ENO/1LNO

SL and $200 \text{ K} \leq T \leq 230 \text{ K}$ for 2ENO/1LNO SL (see Appendix: Fig. 6). Such classical percolation picture has been reported in other oxides as well when they undergo normal to superconducting phase transition^{47,48}. It can be seen from Fig. 3 that the magnitude of noise of 1ENO/1LNO is three orders larger than that of 2ENO/1LNO. Large increase in noise have been seen in other oxide undergoing long range charge-ordering transition³⁸. We speculate that because of the absence of long range CO in 2ENO/1LNO SL, noise magnitude is smaller than 1ENO/1LNO SL.

While the origin of noise in metallic phase can be understood from the Dutta-Horn model^{49,50}, such defect scattering based mechanism fails to explain the peculiar behavior of noise in the temperature range $0.85 \lesssim T/T_{MIT} \lesssim 1.1$ region. To gain better understanding of the origin of such excess noise, we have investigated higher order statistics of resistance fluctuations, which have been used to study the presence of long-range correlations undergoing magnetic, spin-glass⁵², superconducting transition⁴⁸. To calculate the higher order statistics of resistance fluctuations, we have computed the second spectrum. The second spectrum is a four-point correlation function of the resistance fluctuations over a chosen octave (f_l, f_h) and is defined as $S_R^{f_1}(f_2) = \int_0^\infty \langle \delta R^2(t) \rangle \langle \delta R^2(t + \tau) \rangle \cos(2\pi f_2 \tau) d\tau$ where f_1 is the centre frequency of a chosen octave and f_2 is the spectral frequency. Physically, $S_R^{f_1}(f_2)$ represents the ‘spectral wandering’ or fluctuations in the PSD with time in the chosen frequency octave⁵³. To avoid artifacts in the actual signal from the Gaussian background noise, we have calculated the second spectrum over the frequency octave 0.09375-0.1875 Hz, where the sample noise is significantly higher than the background noise. We show plot of the variation of second spectrum $S_R^{f_1}(f_2)$ with of frequency at different T for both superlattices in Appendix (Fig. 7). A convenient way of representing the second spectrum is through the normalized form $\sigma^{(2)}$ defined as $\sigma^{(2)} = \int_0^{f_h-f_l} S_R^{f_1}(f_2) df_2 / [\int_{f_l}^{f_h} S_R(f) df]^2$. For Gaussian fluctuations, $\sigma^{(2)} = 3$ and any deviation from this value would imply the presence of NGC in the fluctuation spectrum⁵³. As expected, $\sigma^{(2)} \sim 3$ in metallic phase of both samples (Fig. 4(a) and (b)). $\sigma^{(2)}$ starts to deviate from 3 for both samples around T_{MIT} , implying that the observation of excess noise is intimately connected to the electronic phase separation. In case of 1ENO/1LNO SL, $\sigma^{(2)}$ shows a peak near $T \sim T_{MIT} = T_N$. On the contrary, $\sigma^{(2)}$ becomes maximum near $T \sim T_N$ for 2ENO/1LNO SL. This surprising observation is likely to be related to the multi-band nature of these materials. The Fermi surface of the paramagnetic metallic phase consists of large hole pockets with small electron pockets⁵⁴. As inferred from the Hall effect measurements by Ojha et al.⁴², the metal insulator transition results in a partially gapped Fermi surface and the hole Fermi surface vanishes around T_N by the nesting driven paramagnetic to E' -antiferromagnetic transition.

The length scale associated with the electronic phase separation can be estimated if we consider that the activation energy (E_a) corresponds to the pure elastic energy generated due to the volume difference between metallic and insulating

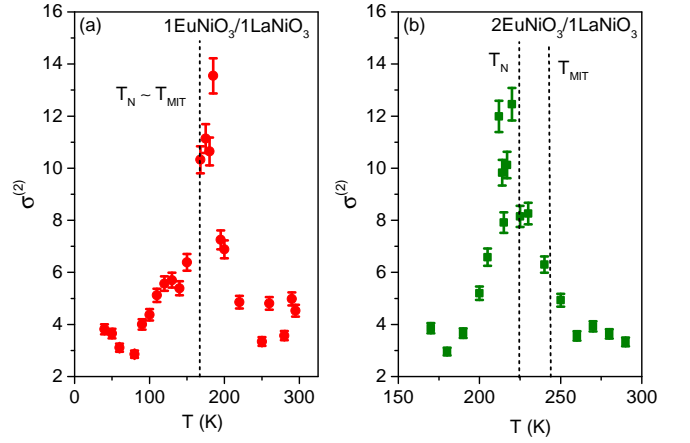


FIG. 4. (a) and (b) Plot of normalized second spectrum $\sigma^{(2)}$ as a function of temperature of 1EuNiO₃/1LaNiO₃ and 2EuNiO₃/1LaNiO₃ respectively.

phase³⁸. The bulk modulus of EuNiO₃ and LaNiO₃ is approximately 320 GPa and 380 GPa, respectively⁵⁵. The out-of-plane lattice constant of the SLs shows around 0.2% expansion across the MIT²¹, yielding an energy density (E_v) ~ 160 -190 kJ/m³ associated with the transformation. By assuming that the metallic nucleating regions are spherical with a diameter L_m , $E_a \sim 0.42 \text{ eV}$ corresponds to $L_m \sim 7.0$ -7.4 nm. We note that conductive-atomic force microscopy study with a spatial resolution of $\sim 100 \text{ nm}$ has found nucleation of metallic domains with size ~ 100 -300 nm in a NdNiO₃ thin film⁵⁶. Our results emphasizes that nucleation of such metallic phase happens at much shorter length scale.

Earlier X-ray absorption spectroscopy experiment demonstrated the presence of short-range charge ordering even in metallic phase of all $RENiO_3$ ⁴⁴. Our present noise measurements emphasize similar characteristics for both samples, such as random resistance fluctuations, $1/f$ noise for $T > T_{MIT}$ and RTN in resistance fluctuations, non- $1/f$ and non-Gaussian characterization of noise for $T > 0.85T_{MIT}$. Further, the very similar length scale associated with nucleation of metallic clusters in the insulating phase in both samples also suggests that the samples have similar electronic and magnetic properties in nanoscale. However, the much smaller noise magnitude of 2ENO/1LNO around T_{MIT} compared to 1ENO/1LNO SL, and additional noise peak near T_N infer that the details of the electrical transport process depend on the presence/absence of long-range charge and magnetic orderings. Complimentary microscopy experiments with sub-nm resolution should help to clarify the details of the development of long-range charge ordered phase from a short-range charge ordered phase and the magnetic nature of phase separated phases around the transition temperatures.

IV. CONCLUSION

To summarize, we have observed the presence of large excess noise around the metal-insulator and magnetic transitions in $\text{EuNiO}_3/\text{LaNiO}_3$ thin films. The appearance of RTN, causing non- $1/f$ noise below T_{MIT} implies that the electronic phase separation is responsible for the excess noise. This is further corroborated by the observation of a large non-Gaussian noise in the insulating phase. Noise in the metallic phase shows $1/f$ behavior with the Gaussian statistics of the resistance fluctuations. Observation of the maxima of $\sigma^{(2)}$ near the T_N for 2ENO/1LNO SL is likely to be connected to the Fermi surface nesting driven origin of E' -type antiferromagnetic ordering. Our experiments highlight the importance of resistance fluctuations study near the phase transition which can be applied to understand transition between two electronic phases of any system.

V. ACKNOWLEDGEMENTS

SM acknowledges IISc start up grant and DST Nanomission grant no. DST/NM/NS/2018/246 for financial support. AB thanks SERB, DST for financial support. J.C. is supported by the Gordon and Betty Moore Foundation EPiQS Initiative through Grant No. GBMF4534.

APPENDIX

To compare the noise level of $\text{EuNiO}_3/\text{LaNiO}_3$ with other nickelates, we have calculated the Hooke parameter γ_H ⁴³, defined as $\gamma_H = \frac{N \times f \times S_R(f)}{R^2}$ (N , total number of charge carriers has been evaluated from Hall effect measurement). The value of γ_H for different nickelates have been tabulated in table I. The large value of γ_H suggests that the origin of noise of these RENiO_3 are different from the scattering mechanism

of electron with lattice phonon mode predicted by Hooke for metals and semiconductors⁴⁵. A possible explanation of large increase in noise is the classical percolation of electrons in inhomogeneous medium⁴⁶.

TABLE I. Value of Hooke parameter for different nickelates at 300 K.

System	Hooke parameter at 300 K
$1\text{EuNiO}_3/1\text{LaNiO}_3$	10^4
$2\text{EuNiO}_3/1\text{LaNiO}_3$	10^4
$\text{LaNiO}_{3-\delta}$ ⁵⁷	10^3
SmNiO_3 ³⁵	5×10^3
NdNiO_3 ^{36,37}	5×10^6

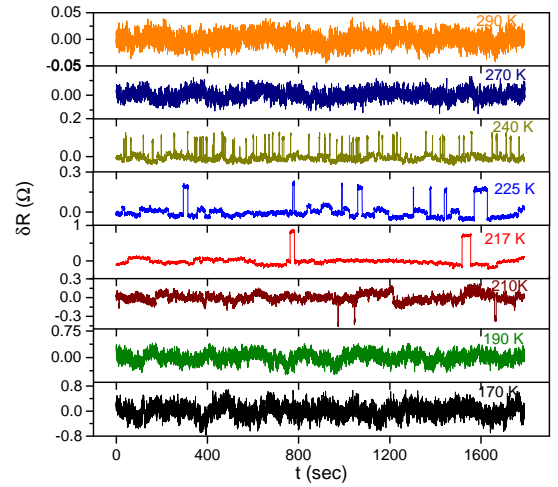


FIG. 5. Time series of resistance fluctuations at few representative values of T of $2\text{EuNiO}_3/1\text{LaNiO}_3$.

* aveek@iisc.ac.in

† smiddey@iisc.ac.in

¹ M. Imada, A. Fujimori, and Y. Tokura, *Rev. Mod. Phys.* **70**, 1039 (1998).

² Y. Tokura, *Reports on Progress in Physics* **69**, 797 (2006).

³ S. Middey, J. Chakhalian, P. Mahadevan, J. W. Freeland, A. J. Millis, and D. D. Sarma, *Annual Review of Materials Research* **46**, 305 (2016).

⁴ S. Catalano, M. Gibert, J. Fowlie, J. Íñiguez, J.-M. Triscone, and J. Kreisel, *Reports on Progress in Physics* **81**, 046501 (2018).

⁵ M. L. Medarde, *Journal of Physics: Condensed Matter* **9**, 1679 (1997).

⁶ G. Catalan, *Phase Transitions* **81**, 729 (2008).

⁷ A. Mercy, J. Bieder, J. Íñiguez, and P. Ghosez, *Nature Communications* **8**, 1667 (2017).

⁸ M. K. Stewart, J. Liu, M. Kareev, J. Chakhalian, and D. N. Basov, *Phys. Rev. Lett.* **107**, 176401 (2011).

⁹ U. Staub, G. I. Meijer, F. Fauth, R. Allenspach, J. G. Bednorz, J. Karpinski, S. M. Kazakov, L. Paolasini, and F. d'Acapito, *Phys. Rev. Lett.* **88**, 126402 (2002).

¹⁰ I. I. Mazin, D. I. Khomskii, R. Lengsdorf, J. A. Alonso, W. G. Marshall, R. M. Ibberson, A. Podlesnyak, M. J. Martínez-Lope, and M. M. Abd-Elmeguid, *Phys. Rev. Lett.* **98**, 176406 (2007).

¹¹ S. R. Barman, A. Chainani, and D. D. Sarma, *Phys. Rev. B* **49**, 8475 (1994).

¹² T. Mizokawa, D. I. Khomskii, and G. A. Sawatzky, *Phys. Rev. B* **61**, 11263 (2000).

¹³ H. Park, A. J. Millis, and C. A. Marianetti, *Phys. Rev. Lett.* **109**, 156402 (2012).

¹⁴ S. Johnston, A. Mukherjee, I. Elfimov, M. Berciu, and G. A. Sawatzky, *Phys. Rev. Lett.* **112**, 106404 (2014).

¹⁵ A. Subedi, O. E. Peil, and A. Georges, *Phys. Rev. B* **91**, 075128 (2015).

¹⁶ V. Bisogni, S. Catalano, R. J. Green, M. Gibert, R. Scherwitzl, Y. Huang, V. N. Strocov, P. Zubko, S. Balandeh, J.-M. Triscone,

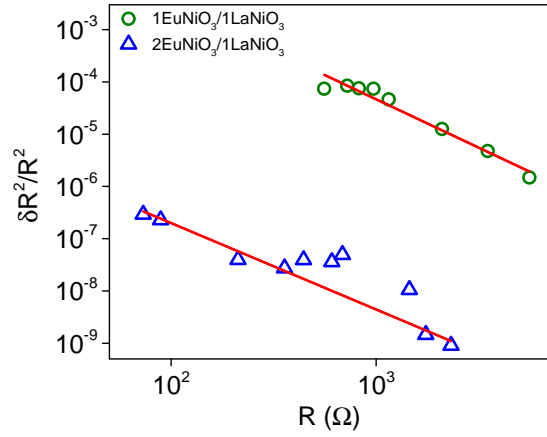


FIG. 6. Log-log plot of $\frac{\delta R^2}{R^2}$ as a function of resistance of 1EuNiO₃/1LaNiO₃ and 2EuNiO₃/1LaNiO₃ respectively. The red line represents the linear fit of the data of slope 2 ± 0.1 . For details see text.

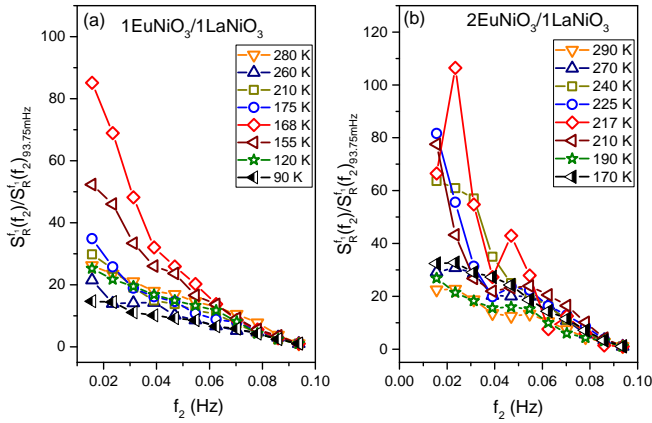


FIG. 7. (a) and (b) Plot of second spectrum $S_R^{f1}(f_2)$ as a function of frequency at different T for 1EuNiO₃/1LaNiO₃ and 2EuNiO₃/1LaNiO₃, respectively. Note that the data have been scaled at 93.75 mHz to see the nature at different temperatures.

- and et al., *Nature Communications* **7**, 13017 (2016).
- ¹⁷ J. Shamblin, M. Heres, H. Zhou, J. Sangoro, M. Lang, J. Neuefeind, J. A. Alonso, and S. Johnston, *Nature Communications* **9**, 86 (2018).
- ¹⁸ S. Lee, R. Chen, and L. Balents, *Phys. Rev. Lett.* **106**, 016405 (2011).
- ¹⁹ S. Lee, R. Chen, and L. Balents, *Phys. Rev. B* **84**, 165119 (2011).
- ²⁰ M. Hepting, M. Minola, A. Frano, G. Cristiani, G. Logvenov, E. Schierle, M. Wu, M. Bluschke, E. Weschke, H.-U. Habermeyer, E. Benckiser, M. Le Tacon, and B. Keimer, *Phys. Rev. Lett.* **113**, 227206 (2014).
- ²¹ S. Middey, D. Meyers, M. Kareev, Y. Cao, X. Liu, P. Shafer, J. W. Freeland, J.-W. Kim, P. J. Ryan, and J. Chakhalian, *Phys. Rev. Lett.* **120**, 156801 (2018).
- ²² R. Scherwitzl, P. Zubko, I. Gutierrez Lezama, S. Ono, A. F. Morpurgo, G. Catalan, and J. M. Triscone, *Advanced Materials*, **22**, 5517 (2010).

- ²³ J. Shi, S. D. Ha, Y. Zhou, F. Schoofs, and S. Ramanathan *Nat. Commun.* **4**, 2676 (2013).
- ²⁴ J. Shi, Y. Zhou and S. Ramanathan, *Nat. Commun.* **5**, 4860 (2014).
- ²⁵ S. D. Ha, J. Shi, Y. Meroz, L. Mahadevan, and S. Ramanathan, *Phys. Rev. Appl.* **2**, 064003 (2014).
- ²⁶ B. K. Jones - *IEE Proceedings-Circuits, Devices and Systems*, **149**, 13 (2002).
- ²⁷ R. Koushik, M. Baenninger, V. Narayan, S. Mukerjee, M. Pepper, I. Farrer, D. A. Ritchie, and A. Ghosh, *Physical Review B* **83**, 085302 (2011).
- ²⁸ U. Chandni, A. Ghosh, H. Vijaya, and S. Mohan, *Physical review letters* **102**, 025701 (2009).
- ²⁹ H. K. Kundu, S. Ray, K. Dolui, V. Bagwe, P. R. Choudhury, S. Krupanidhi, T. Das, P. Raychaudhuri, and A. Bid, *Physical review letters* **119**, 226802 (2017).
- ³⁰ J. Clarke and T. Y. Hsiang, *Physical Review B* **13**, 4790 (1976).
- ³¹ D. Babić, J. Bentner, C. Sürgers, and C. Strunk, *Physical Review B* **76**, 134515 (2007).
- ³² F. Reif, *Fundamentals of statistical and thermal physics*, Waveland Press (2009).
- ³³ M. B. Weissman, *Rev. Mod. Phys.* **60**, 537 (1988).
- ³⁴ A. Ghosh, S. Kar, A. Bid, and A. Raychaudhuri, *arXiv preprint cond-mat/0402130* (2004).
- ³⁵ A. Sahoo, S. D. Ha, S. Ramanathan, and A. Ghosh, *Physical Review B* **90**, 085116 (2014).
- ³⁶ A. M. Alsaqqa, S. Singh, S. Middey, M. Kareev, J. Chakhalian, and G. Sambandamurthy, *Physical Review B* **95**, 125132 (2017).
- ³⁷ R. S. Bisht, S. Samanta, and A. K. Raychaudhuri, *Phys. Rev. B* **95**, 115147 (2017).
- ³⁸ A. Bid, A. Guha, and A. Raychaudhuri, *Physical Review B* **67**, 174415 (2003).
- ³⁹ S. Middey, D. Meyers, M. Kareev, X. Liu, Y. Cao, J. W. Freeland, and J. Chakhalian, *Phys. Rev. B* **98**, 045115 (2018).
- ⁴⁰ S. Middey, D. Meyers, R. K. Patel, X. Liu, M. Kareev, P. Shafer, J.-W. Kim, P. J. Ryan, and J. Chakhalian, *Applied Physics Letters* **113**, 081602 (2018).
- ⁴¹ J.-S. Zhou, J. B. Goodenough, and B. Dabrowski, *Phys. Rev. Lett.* **94**, 226602 (2005).
- ⁴² S. K. Ojha, S. Ray, T. Das, S. Middey, S. Sarkar, P. Mahadevan, Z. Wang, Y. Zhu, X. Liu, M. Kareev, and J. Chakhalian, *Phys. Rev. B* **99**, 235153 (2019).
- ⁴³ F. N. Hooge, *Phys. Lett.* **29**, 139 (1969).
- ⁴⁴ C. Piamonteze, H. C. N. Tolentino, A. Y. Ramos, N. E. Massa, J. A. Alonso, M. J. Martínez-Lope, and M. T. Casais, *Phys. Rev. B* **71**, 012104 (2005).
- ⁴⁵ F. N. Hooge, *Physica* **60**, 130 (1972).
- ⁴⁶ A.-M. S. Tremblay, S. Feng, and P. Breton, *Phys. Rev. B* **33**, 2077 (1986).
- ⁴⁷ L. B. Kiss and P. Svedlindh, *IEEE Transactions on Electron Devices* **41**, 2112 (1994).
- ⁴⁸ G. N. Daptary, S. Kumar, P. Kumar, A. Dogra, N. Mohanta, A. Taraphder, and A. Bid, *Physical Review B* **94**, 085104 (2016).
- ⁴⁹ P. Dutta and P. Horn, *Reviews of Modern physics* **53**, 497 (1981).
- ⁵⁰ G. N. Daptary, C. Sow, S. Sarkar, S. Chiniwar, P. A. Kumar, A. Sil, and A. Bid, *Physica B: Condensed Matter* **511**, 74 (2017).
- ⁵¹ G. Seidler, S. Solin, and A. Marley, *Physical review letters* **76**, 3049 (1996).
- ⁵² G. N. Daptary, C. Sow, P. A. Kumar, and A. Bid, *Physical Review B* **90**, 115153 (2014).
- ⁵³ G. Seidler and S. Solin, *Physical Review B* **53**, 9753 (1996).
- ⁵⁴ R. Eguchi, A. Chainani, M. Taguchi, M. Matsunami, Y. Ishida, K. Horiba, Y. Senba, H. Ohashi, and S. Shin, *Phys. Rev. B* **79**, 115122 (2009).

- ⁵⁵ J.-S. Zhou, J. B. Goodenough, and B. Dabrowski, *Phys. Rev. B* **70**, 081102 (2004).
- ⁵⁶ D. Preziosi, L. Lopez-Mir, X. Li, T. Cornelissen, J. H. Lee, F. Trier, K. Bouzehouane, S. Valencia, A. Gloter, A. Barthlmy, *et al.*, *Nano letters* **18**, 2226 (2018).
- ⁵⁷ A. Ghosh, A. K. Raychaudhuri, R. Sreekala, M. Rajeswari, and T. Venkatesan, *Journal of Physics D: Applied Physics*, **30**, L75 (1997).